Numerical Simulation of Nasal Resistance Using Three-dimensional Models of the Nasal Cavity and Paranasal Sinus

Shoji KANEDA[*1], Fumiyuki GOTO[*1], Kenji OKAMI[*1],
Reo MITSUTANI[*2] and Yoko TAKAKURA[*2]

[*1] *Department of Otolaryngology, Head and Neck surgery, Tokai University School of Medicine*
[*2] *Course of Science and Technology, Tokai University*

(Received December 8, 2022; Accepted February 6, 2023)

Objective: Previously, we used a nasal cavity model to analyze the intranasal airflow dynamics and numerically calculate the nasal resistance value. In this study, We attempted clarify the parameters influencing nasal resistance by newly developed computer model.
Methods: The computer simulation model was developed from the structures of nasal airway tract adopted from 1.0-mm slice computed tomography (CT) obtained from the 2 of the healthy volunteers. (model 1: the one at 35-year-old man, model 2: 25-year-old man. We have calculated the nasal resistance by computer simulation calculations of both model 1 and model 2. These calculated values were compared with the values obtained from the established method of rhinomanometry.
For the simulation, Fluent 17.2® (ANSYS, American) was employed for fluid analysis using the continuity equation for 3D incompressible flow and the Navies–Stokes equation for the basic equations. Both models were laminar models. The SIMPLE calculation method using the finite volume method was employed here, and the quadratic precision upwind difference method was used to discretize the convection terms.
Results: The measured (simulation) values in Model 1 were 0.69 (0.48), 1.10 (0.41), and 0.42 (0.22) Pa/cm^3/s on the right, left, and both sides, whereas those in Model 2 were 0.72 (0.21), 0.32 (0.09), and 0.22 (0.06) Pa/cm^3/s, respectively.
Conclusion: Our results suggest that nasal resistance is possibly affected by the length of the inferior turbinate and the cross-sectional area of the choana and nasopharynx. Further experiments using additional nasal cavity and paranasal sinus models are warranted.

Key words: nasal cavity, paranasal sinuses, turbinate, rhinomanometry, tomography, computer simulation

INTRODUCTION

Several patients with rhinology diseases experience nasal obstruction. The nasal obstruction is common clinical problem because approximately 40% of allergic rhinitis patients have nasal obstruction [1]. For evaluating nasal obstruction, rhinomanometry is popular worldwide [2]. Rhinomanometry can determine nasal pressure and airflow during inspiration and expiration. Additionally, it can measure nasal resistance to measure the pressure difference between the nostril and choana. Nasal resistance can be affected by alternating congestion and decongestion of the nasal mucosa, which is termed the nasal cycle [3, 4]. Lang *et al*. investigated the nasal cycle using endoscopy, rhinoresistometry, and acoustic rhinometry [5]. Gogniashvili *et al*. also investigated the nasal cycle in the same manner [6]. In general anesthesia, nasal patency is investigated before nasal intubation [7]. Rhinomanometry can measure nasal resistance during the nasal cycle; however, it cannot measure the direct airflow pressure in the nasal cavity.

Recently, computational fluid dynamics (CFD) in rhinology has become popular for measuring airflow or pressure [8, 9]. This enables the observation of the airflow, pressure, heat, and streamline, which cannot be determined directly using computer simulation. Kim *et al*. reviewed patient-specific CFD models of nasal airflow [10]. Moreover, Wang *et al*. simulated applying CFD to the study of the nasal cavity in 2005 [11]. In turn, Xiong *et al*. reported a numerical flow simulation in virtual post-endoscopic sinus surgery [12]. Twenty-two healthy adults were studied to determine the normal nasal airflow [13]. It was found that nasal resistance affected nasal obstruction. Recently, these phenomena were simulated using CFD. Radulesco reported a comparison of nasal obstruction with CFD variables [14]. Finally, Berger reported the agreement between rhinomanometry and CFD regarding nasal resistance [15].

CFD can be achieved by creating a three-dimensional (3D) model and using numerical simulation. However, the nose is composed of the nasal cavity and paranasal sinuses and is a very complicated structure. Thus, it is very difficult to create a highly accurate 3D model of the nasal cavity and paranasal sinuses. The recent literature includes many CFD rhinology documents, with the absence of accurate nose 3D models.

Shoji KANEDA, Department of Otolaryngology, Head and Neck Surgery, Tokai University School of Medicine, 143 Shimokasuya, Isehara, Kanagawa 259-1193, Japan Tel: +81-463-93-1121 Fax: +81-463-94-1611 E-mail: s.kaneda@tokai.ac.jp

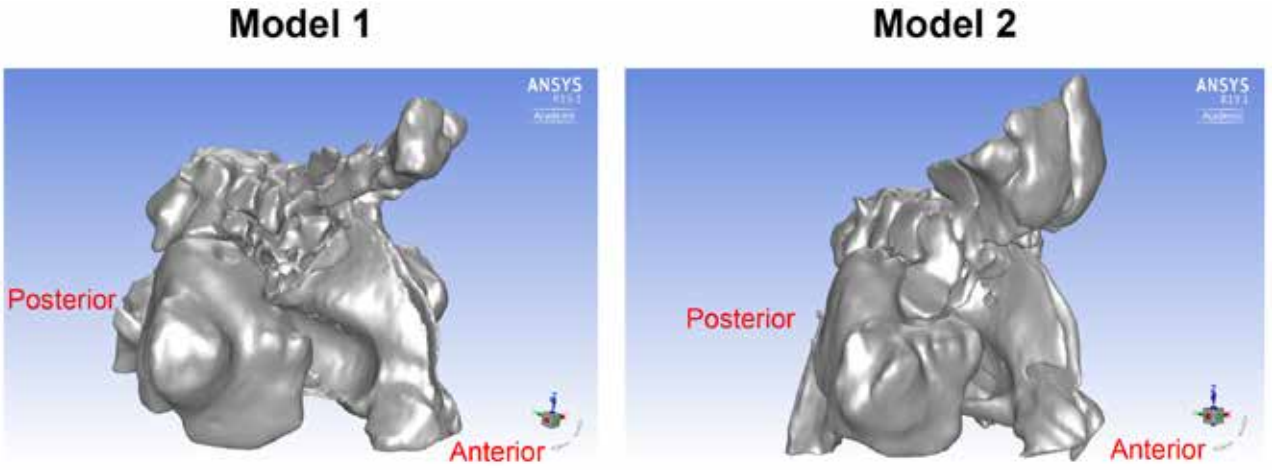

Fig. 1 Findings from Models 1 and 2

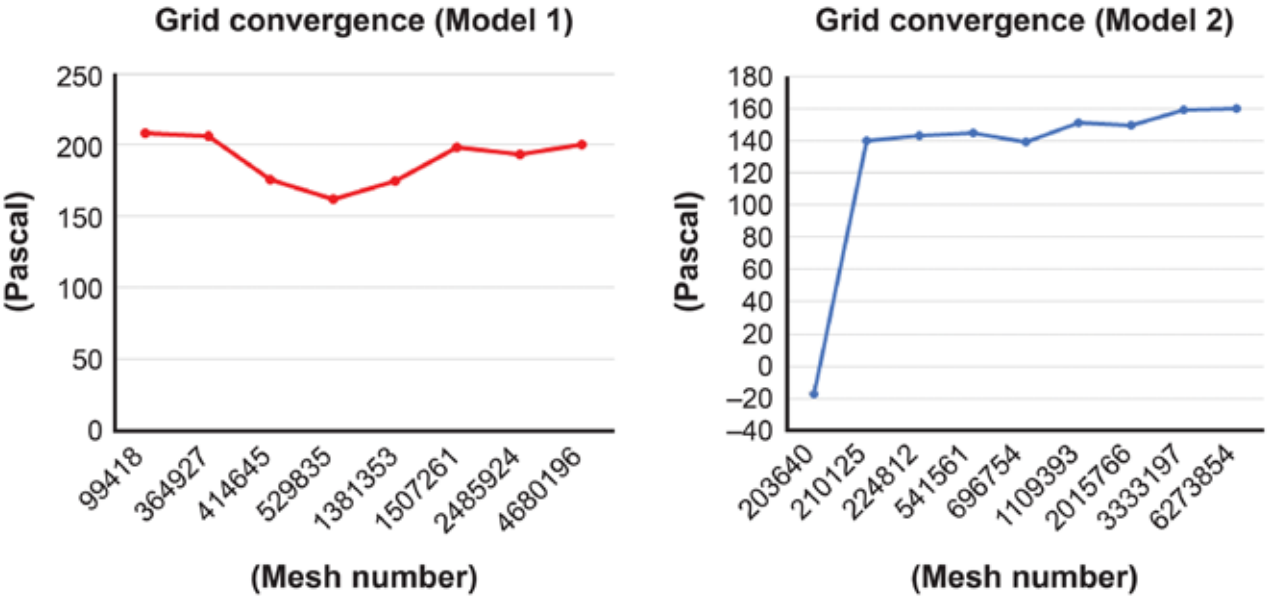

Fig. 2 Grid Convergence of Models 1 and 2

Therefore, we created a 3D model of the nose to check the all-natural ostium of all paranasal sinuses. It was unclear whether the simulation in reality reflected the human body. By comparing the real nasal resistance value, which can be measured, with the numerical simulation value, it is possible to judge whether or not it is closer to the human body.

In this research, we compared the measured and calculated nasal resistance values using the newly created nasal cavity and paranasal sinus model. We streamlined these data and studied the relationship between the model and nasal resistance and tried to validate the factors that affect the nasal resistance from the 3D CT model.

MATERIALS AND METHODS

Patient Population and Model Generation

Study protocol was approved by IRB with (17R369). All participant gave written informed consent. Three dimensional images of nasal cavity models were constructed to reproduce the model obtained from the 2 of healty volunteers (35-year-old male (Model 1) and a 25-year-old male (Model 2)). The models were adopted from the structures taken as images with a width of 1.0 mm and a pixel size of 0.488 mm × 0.488 mm × 0.488 mm by scanned using a computed tomography (CT) instrument (SIEMENS SOMATOM Definition Edge®, Germany). The cavity and paranasal sinus 3D model was created using Mimics 23.0® (Materialize, Belgium) (Fig. 1).

Model Refinement

The 3-matic 15.0® (Materialize, Belgium) was used for mesh formation after the smoothing procedure. The TetGen mesh generator was used here with the boundary condition that the boundary surface must remain intact (unchanged), both at the vertices and triangles. This means that if tetrahedron vertices (called Steiner points in Delauney terminology) are to be added by the algorithm, they are never added at the boundary surface, but only at the interior of the model. The number of surface meshes was 177448 in Model 1 and 136332 in Model 2. The number of volume meshes was 353933 in Model 1 and 285874 in Model 2. The number of nodes was 103629 in Model 1 and 82312 in Model 2. The grid convergence of these

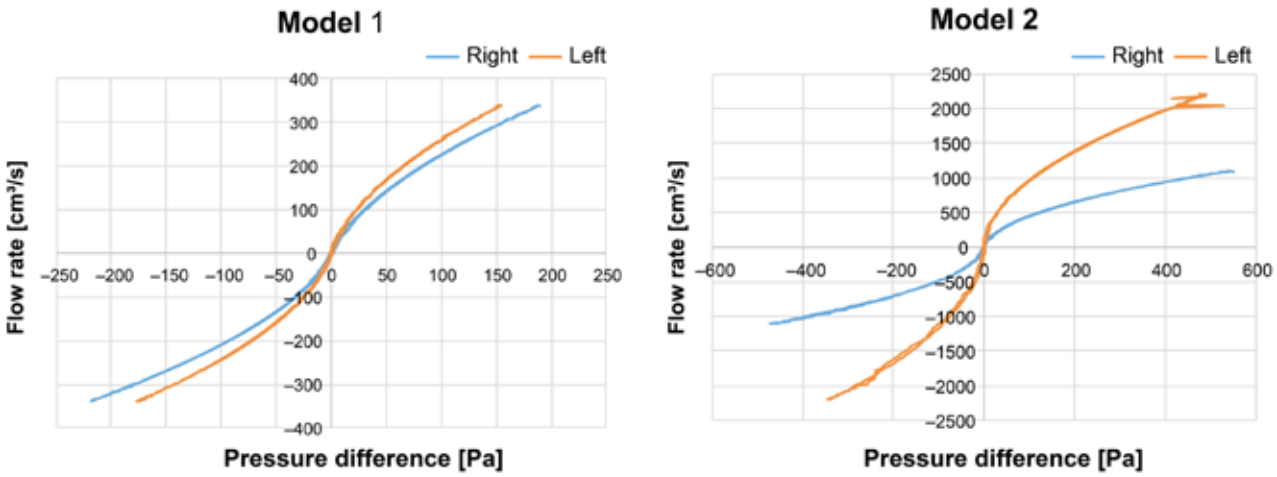

		Simulation	Measurement
Model 1	Right	0.48	0.69
	Left	0.41	1.10
	Both	0.22	0.42
Model 2	Right	0.21	0.72
	Left	0.09	0.32
	Both	0.06	0.22

Fig. 3 Results of nasal resistance in Models 1 and 2 in the numerical simulation and the comparison of nasal resistance between the simulation and measurement situations (the value of inspiration Δ100 Pa of nasal resistance R [Pa/cm^3/s])

models was calculated. We confirmed that the number of volume meshes of these models were appropriate (Fig. 2).

Simulation Calculation

The boundary conditions were as follows:

i) The velocity is equal to zero at the nasal wall;

ii) A pressure of zero is presumed at the nostrils as the atmospheric pressure;

iii) At the trachea side, the velocity (v) is given.

In the steady solution, the iteration number was 300. In turn, in the unsteady solution, the iteration number was 20/time step and the time step width was 0.001 [s]. We used a sine function of 3 s per period as the breath airflow.

The nasal resistance value, R (Pa/[cm^3/s]), was calculated by the following formula using the flow rate V (cm^3/s) at the nostril when the pressure difference (ΔP) between the atmospheric pressure and the pharynx was 100 (Pa):

$R = \Delta P/V$,

where R is the nasal resistance (Pa/[cm^3/s]), ΔP is the differential pressure between the atmospheric pressure and the pharynx (Pa), and V is the flow rate (cm^3/s).

After the calculation of the resistance for each cavity, the right (R_{right}) and left resistance (R_{left}) were calculated, with the total resistance for both cavities, R_{total}, being calculated as follows:

$1/R_{total} = 1/R_{right} + 1/R_{left}$.

First, we performed a simulation with a flow velocity of 1.5 (m/s) applied to the pharyngeal side in the steady solution. A pressure difference of Δ100 (Pa) was required to measure the nasal resistance value. Second, we performed a simulation in the same condition using the unsteady solution for the nasal resistance. The maximum flow velocity in Model 1 was 1.5 (m/s) on the right and 1.5 (m/s) on the left. Moreover, in Model 2, the maximum flow velocity was 3.0 (m/s) on the right and 6.0 (m/s) on the left in the unsteady solution.

Rhinometry was performed using an MPR-3100® instrument (Nihonkoden, Japanese). Nasal resistance was measured in the two subjects using active anterior rhinometry (without vasoconstriction). To rule out the effect of the nasal cycle, nasal resistance was measured right after CT.

Ethical consideration

The authors assert that all procedures contributing to this work comply with the ethical standards of the relevant national and institutional guidelines on human experimentation (the Ethical Committee of Tokai University [approval number: 17R369 in 2018]) and with the Helsinki Declaration of 1975, as revised in 2008.

Reporting guidelines

STROBE checklist (for observational studies) was followed for this study.

RESULTS

The simulation values were obtained in an unsteady solution. The nasal resistance measured (simulation) values of Model 1 were 0.69 (0.48) on the right, 1.10 (0.41) on the left, and 0.42 (0.22) on both sides. The actual measurement (simulation) values of Model 2 were 0.72 (0.21) on the right, 0.32 (0.09) on the left,

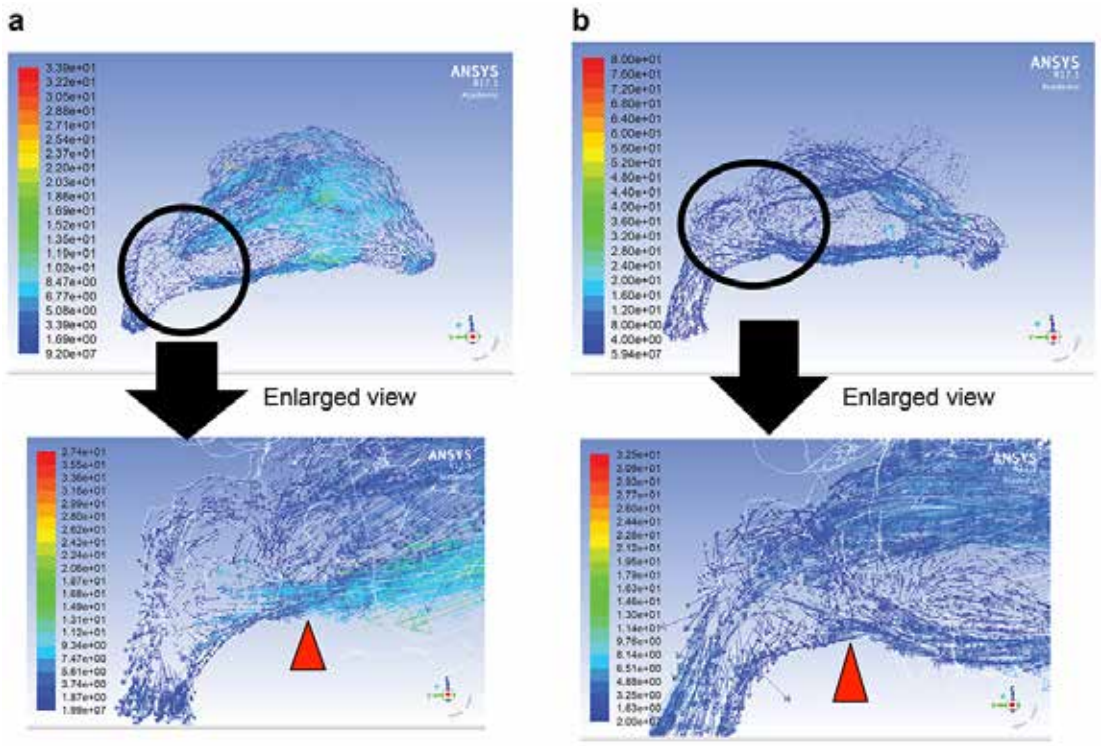

Fig. 4 Velocity vector of Models 1 and 2
(a) Velocity vector of Model 1. The speed suddenly decreased near the choana (△).
(b) Velocity vector of Model 2. The speed remained unchanged compared with Model 1 (△).

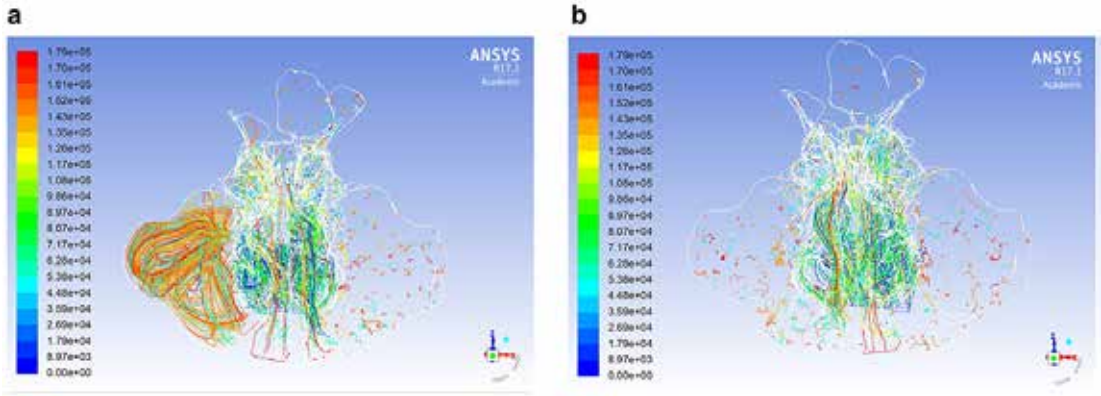

Fig. 5 Streamlining of Model 1; view from the front
(a) Right open streamline. Ventilation in the maxillary sinus and ethmoidal sinus; however, ventilation in the frontal sinus was not observed.
(b) Left open streamline. Ventilation of the frontal sinus and maxillary sinus was not observed.

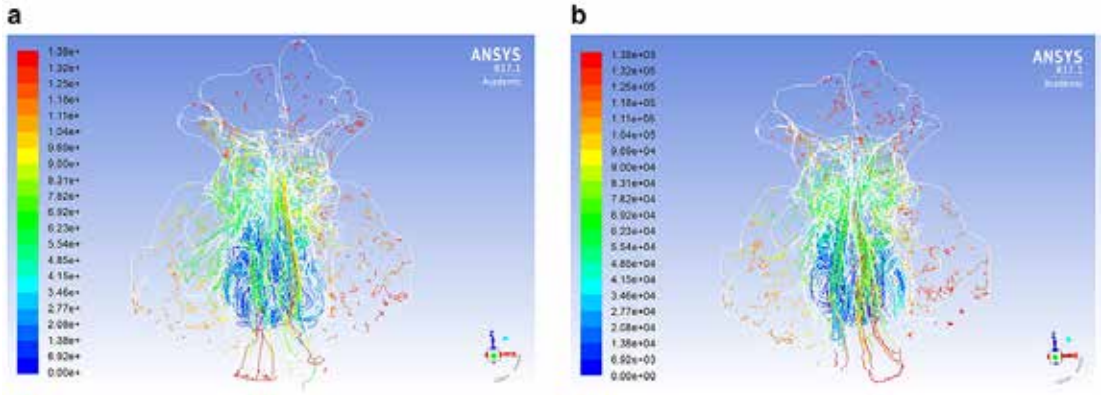

Fig. 6 Streamlining of Model 2; view from the front
(a) Right open streamline. Ventilation of the frontal sinus and maxillary sinus was not observed.
(b) Left open streamline. Ventilation of the frontal sinus and maxillary sinus was not observed.

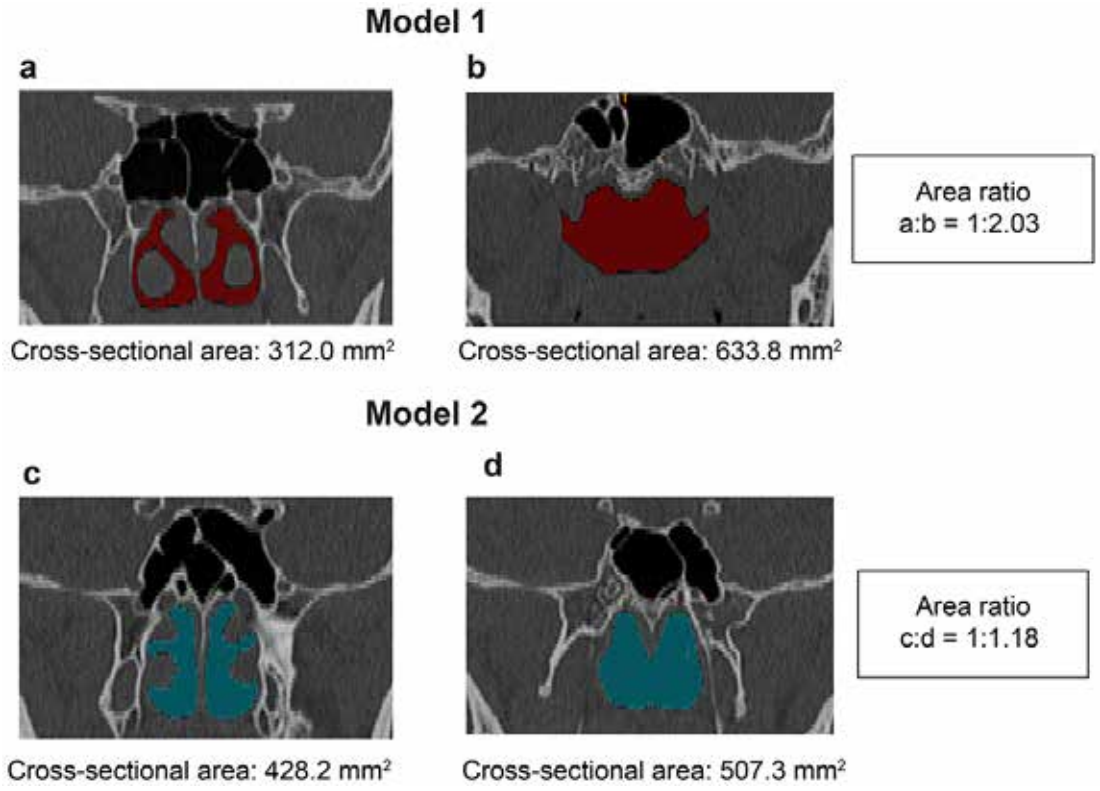

Fig. 7 Area of the posterior end of the inferior turbinate and nasopharyngeal section of Models 1 and 2
A comparison of the cross-sectional areas showed that the cross-sectional areas of Model 1 have changed significantly.

and 0.22 (0.06) on both sides (Fig. 3).

Additionally, the velocity vector of Models 1 and 2, as assessed using a steady-state calculation, is shown in Fig. 4. The speed near the choana was suddenly reduced in Model 1. Conversely, the speed remained unchanged in Model 2.

The streamlining of Models 1 and 2 using a steady-state calculation is shown in Fig. 4 and 5. In Model 1, we observed ventilation in the right maxillary sinus and in both ethmoidal sinuses. Conversely, we did not observe ventilation in the left maxillary sinuses or in both frontal sinuses (Fig. 5). Additionally, in Model 2, we did not observe ventilation in the frontal and maxillary sinuses (Fig. 6).

DISCUSSION

Two accurate nasal cavity and paranasal sinus models were created, and numerical simulation of nasal ventilation was performed. In our research, in the simulation that was performed using the nasal cavity model without the sinuses, the magnitude of the relationship was correct, but the simulation value tended to be lower than the actual measurement, although a similar tendency was observed [16]. By including the paranasal sinuses, the simulation was expected to approach the measured value because it would be closer to the actual shape; however, this was not the case. This discrepancy can be attributed to the fact that the airflow in the model shown in Figure 5 hardly entered the paranasal sinuses.

There are two possible explanations for the observation that Model 1 had a higher nasal resistance value than Model 2. 1) In Model 1, the cross-sectional area became smaller than that of Model 2 as it approached the choana; thus, the flow velocity increased from the continuity equation. As the flow velocity increased, the pressure decreased based on Bernoulli's principle.

2) The difference in the cross-sectional areas of the nasopharynx compared with the choana was larger in Model 1 than in Model 2. Thus, an energy loss occurred because of the reverse pressure gradient due to the rapid expansion of the cross-sectional area; it became a pressure loss, and the pressure drop became even larger (Fig. 7).

Ventilation into the sinuses remains uncertain, but it is unlikely that there is no ventilation. In our study, Model 1 exhibited ventilation in the maxillary and ethmoidal sinuses exclusively. Kumar *et al.* reported the air flow in the periods pre- and post-endoscopic sinus surgery using numerical simulation [17]. However, the 3D model reported by them in pre-surgery did not connect the nasal cavity with the frontal sinus and maxillary sinus. Therefore, it was difficult to create an accurate 3D model. The natural ostium connecting the sinuses and the nasal cavity may not be accurately created. To date, it has been reported that the nasal sinus model is used to examine the correlation between the nasal air permeability measurement and the numerical simulation, and although they are similar, they do not completely match [15]. Radulesco *et al.* reported the measured and simulated nasal resistance before septoplasty using 22 nasal cavity models. The perceptions of the patients and the measured and simulated nasal resistance exhibited strong correlations. However, the measured and simulated nasal resistance were poorly correlated [18]. Tretiakow *et al.* investigated the workflow for creating a 3D model for accurate CFD [19]. We think that it is necessary to create an accurate

nasal sinus model for more accurate simulation.

Our results suggest that the length of the inferior turbinate and the cross-sectional area of the nasopharynx and the choana affect the nasal resistance value. Hariri *et al*. reported that inferior turbinate weight loss reduced nasal resistance in 3 of 5 models, whereas it remained unchanged in the two remaining models. In the two cases without change, the nasal resistance was affected by factors other than the inferior turbinates [20]. The relationship between the length of the inferior turbinates and the cross-sectional area encompassing the nasopharynx, as in this example, may also affect the nasal resistance value. However, the sample size used in our investigation was two volunteers, which was too small to draw any conclusions on the effect of nasal resistance in this context. A larger sample size is needed for further investigation.

In conclusion, using the two nasal cavity and paranasal sinus models, the nasal resistance value was calculated via numerical simulation. The length of the inferior turbinates and the cross-sectional area of the choana and nasopharynx may affect the nasal resistance. A more accurate model is needed for future simulations.

ACKNOWLEDGMENTS

The authors would like to thank Enago (www.enago.jp) for the English-language review.

REFERENCES

1) Osborn JL, Sacks R. Nasal obstruction. Am J Rhinol Allergy 2013; Suppl 1 S7–8.
2) Scadding G, Hellings P, Alobid I, Bachert C, Fokkens W, van Wijk RG, *et al*. Diagnostic tools in Rhinology EAACI position paper. Clin Transl Allergy 2011; 1: 2.
3) Hasegawa M, Kern EB. Variations in nasal resistance in man: a rhinomanometric study of the nasal cycle in 50 human subjects. Rhinology 1978; 16: 19–29.
4) Eccles R. Nasal airflow in health and disease. Acta Oto-Laryngol 2000; 120: 580–95.
5) Lang C, Grützenmacher S, Mlynski B, Plontke S, Mlynski G. Investigating the nasal cycle using endoscopy, rhinoresistometry, and acoustic rhinometry. Laryngoscope 2003; 113: 284–9.
6) Gogniashvili G. Sh J, Khujadze M. Investigation of the nasal cycle function through endoscopy, rhinoresistometry, and acoustic rhinometry. Georgian News 2009; 174: 22–5.
7) Shohara K, Goto T, Kuwahara G, Isakari Y, Moriya T, Yamamuro T. Validity of rhinometry in measuring nasal patency for nasotracheal intubtion. J Anesth 2017; 31: 1–4.
8) Wong E, Inthavong K, Singh N. Comment on the European position paper on diagnostic tools in rhinology â€"computational fluid dynamics. Rhinology 2019; 57: 477–8.
9) Quadrio M, Pipolo C, Corti S, Lenzi R, Messina F, Pesci C, *et al*. Review of computational fluid dynamics in the assessment of nasal air flow and analysis of its limitations. Eur Arch Otorhinolaryngol 2014; 271: 2349–54.
10) Kim SK, Na Y, Kim JI, Chung SK. Patient specific CFD models of nasal airflow: overview of methods and challenges. J Biomech 2013; 46: 299–306.
11) Wang K, Denney TS, Morrison EE, Vodyanoy VJ. Numerical simulation of air flow in the human nasal cavity. Conf Proc IEEE Eng Med Biol Soc 2005; 2005: 5607–10.
12) Xiong G, Zhan J, Zuo K, Li J, Rong L, Xu G. Numerical flow simulation in the post-endoscopic sinus surgery nasal cavity. Med Biol Eng Comput 2008; 46: 1161–7.
13) Zhao K, Jiang J. What is normal nasal airflow? A computational study of 22 healthy adults. Int Forum Allergy Rhinol 2014; 4: 435–46.
14) Radulesco T, Meister L, Bouchet G, Giordano J, Dessi P, Perrier P, *et al*. Functional relevance of computational fluid dynamics in the field of nasal obstruction: a literature review. Clin Otolaryngol 2019; 44: 801–9.
15) Berger M, Giotakis AI, Pillei M, Mehrle A, Kraxner M, Kral F, *et al*. Agreement between rhinomanometry and computed tomography-based computational fluid dynamics. Int J Comput Assist Radiol Surg 2021; 16: 629–38.
16) Kaneda S, Iida M, Yamamoto H, Sekine M, Ebisumoto K, Sakai A, *et al*. Evaluation of nasal airflow and resistance: computational modeling for experimental measurements. Tokai J Exp Clin Med 2019; 44: 59–67.
17) Kumar H, Jain R, Douglas RG, Tawhai MH. Airflow in the human nasal passage and sinuses of chronic rhinosinusitis subjects. PLOS ONE 2016; 11: e0156379.
18) Radulesco T, Meister L, Bouchet G, Varoquaux A, Giordano J, Mancini J, *et al*. Correlations between computational fluid dynamics and clinical evaluation of nasal airway obstruction due to septal deviation: an observational study. Clin Otolaryngol 2019; 44: 603–11.
19) Tretialow D, Tesch K. Three-dimensional modeling and automatic analysis of the human nasal cavity and paranasal sinuses using the computational fluid dynamics method. Eur Arch Oto-Rhino-L 2020; 278: 1443–53.
20) Hariri BM, Rhee JS, Garcia GJ. Identifying patients who may benefit from inferior turbinate reduction using computer simulations. Laryngoscope 2015; 125: 2635–41.